# Comparing Hydrogen and Jet-A for an N+3 Turbofan with Water Recirculation using Gradient-Based Optimization

Peter N. Atma*, Andrew H .R. Lamkin†, and Joaquim R. R. A. Martins‡
*University of Michigan, Ann Arbor, MI, 48109*

**Advances in commercial propulsion technology led to the development of efficient high bypass ratio turbofan engines with larger overall pressure ratios and internal temperatures. Current trends suggest that geared ultra high bypass ratio turbofans are the next generation of commercial propulsion systems. Furthermore, the emphasis on decreasing emissions has driven the exploration of hydrogen-powered aircraft, adding to the already challenging design space. Carrying and burning hydrogen introduces complexity and weight penalties that we must offset using the fuel's thermodynamic and chemical properties. In this study, we create a closed-loop water recirculation system with a zero-dimensional thermodynamic model and compare the benefits between Jet-A and hydrogen fuels. We perform a gradient-based optimization parameter sweep to explore the trade-offs between performance and emissions using both fuels with water recirculation. The results quantify the design space for next-generation propulsion concepts that can take advantage of hydrogen fuel's advantageous thermodynamic properties to reduce emissions and improve performance.**

## I. Introduction

The effects of climate change are pushing the aviation industry towards hydrogen-fueled propulsion systems as a solution to reduce emissions. N+3 technology estimates for engines that burn hydrocarbon fuels suggest that higher efficiencies can be achieved by designing ultra high bypass ratio (UHBR) turbofans with small cores and high overall pressure ratios (OPR). Higher OPR and smaller cores challenge the limits of compressor and turbine design, placing an upper bound on potential performance and emissions improvements. Switching to hydrogen as the primary fuel source reduces carbon dioxide emissions immediately, but adds complexity and weight that can offset the benefits [1]. However, hydrogen is a versatile fuel with advantageous molecular and thermodynamic properties that can be exploited to increase the performance and reduce emissions. We introduce a closed-loop water recirculation model that demonstrates the possible efficiency gain when hydrogen is used for purposes other than combustion.

Water injection is the process of introducing water upstream of the combustor as finely atomized droplets. NASA, Boeing, and Rolls-Royce studied this concept and suggested that this technique reduces the NOx emissions as much as 47 percent [2]. Additionally, water injection improves fuel efficiency and thrust output with lower combustion temperatures that can improve the lifetime of turbine blades and reduce noise [2]. Traditional propulsion systems that burn hydrocarbon fuels would require external demineralized water storage on the aircraft for water injection [3]. The added weight of tanks, pumping, and ducting makes this concept infeasible for a conventional aircraft over the entire flight. The main product of hydrogen combustion is water vapor that we can recover from the exhaust stream [4]. Condensing water vapor from the exhaust stream of hydrogen combustion and recirculating it eliminates any additional storage requirements. This allows for the theoretical design of a closed loop water feedback system inside the propulsion cycle. Pratt and Whitney are actively researching this technology to improve the feasibility of hydrogen-powered propulsion [5]. They suggest that water vapor can be recovered by utilizing the thermal properties of hydrogen to condense some of the water in the turbofan exhaust.

Zero-dimensional cycle modeling is an efficient tool for predicting the initial design, performance, and emissions of new propulsion concepts. Zero-dimensional analysis uses a first-principles approach with a chemical equilibrium analysis (CEA) thermodynamics solver [6] that considers the molecular species of different fuels. The industry standard for thermodynamic cycle analysis is the Numerical Propulsion System Simulation (NPSS) framework [7]. NPSS is a modular object-oriented library that models engine components as individual blocks with several thermodynamic solvers. Hendricks and Gray [8] created a new tool called pyCycle with the same functionality as NPSS with analytical

*MSE Student, Department of Aerospace Engineering, AIAA Student Member
†Ph.D. Candidate, Department of Aerospace Engineering, AIAA Student Member
‡Professor, Department of Aerospace Engineering, AIAA Fellow

derivatives [9]. pyCycle is built on top of the OpenMDAO framework [10] to enable gradient-based optimization and leverage hierarchical nonlinear solver structures for robustness.

In this work, we analyze the thermodynamic benefits of a closed-loop water vapor recovery and water injection system in a high-bypass turbofan engine. We develop pyCycle components for water injection and vapor recovery to quantify the benefit of a closed loop recirculation system. We use gradient-based optimization to minimize fuel burn subject to performance requirements using both Jet-A and hydrogen at a range of flight conditions. The optimized results show the trade-off between complexity, performance, and efficiency for Jet-A and hydrogen fuels.

This work is organized as follows. First, in Section II, we introduce the turbofan model and explain the water injection and water recovery components. In section III the implementation of the multipoint optimization problem is discussed. Finally, we present the optimized results and discuss the design space in section IV.

## II. Methodology

The UHB turbofan model is the NASA advanced technology "N+3" engine [11]. The N+3 reference cycle is a UHB ratio geared turbofan that could be available in the 2030 to 2040 time frame. The flow path consists of an inlet that directs ambient air through a fan, followed by a duct that splits the flow into a core and a bypass stream, each ending in a core and bypass nozzle, respectively. The low pressure system is split into two mechanical subsystems. First, the fan is connected to the gearbox that reduces the shaft speed to decrease fan tip speeds. Second, the gearbox attaches to the low-pressure shaft that connects to the low-pressure compressor (LPC) and low-pressure turbine (LPT). The high pressure compressor (HPC) is connected to the high pressure turbine (HPT) by the high pressure shaft. Figure 2 shows a standard high bypass turbofan engine flow connections. We introduce the closed-loop water recovery system as a feedback cycle that transports water from the exhaust to a point upstream of the compressors. The recovery system injects vaporized water into the core stream that reduces the combustion temperature due to heat absorption. The vapor recovery component is placed directly before the core nozzle to extract water from the exhaust and recycles it back to the injector. Figure 4 shows the water vapor recovery loop implemented in a turbofan engine.

In this section we present the full engine layout and provide details on the multipoint zero-dimensional modeling approach. We explain the implementation and assumptions of the water recovery model and the coupling with the thermodynamic cycle.

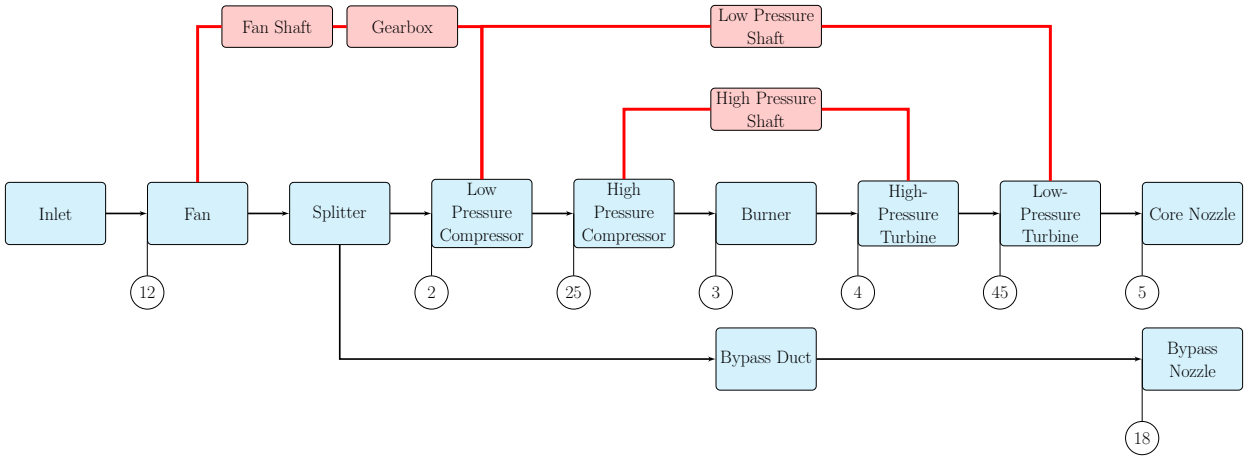


**Fig. 1 Simplified layout of the N+3 engine cycle, adapted from Hendricks and Gray [8]. Black arrows are flow connections, red lines are mechanical connections, blue boxes are cycle elements, red boxes are shaft elements. Flow stations are identified with bubble text.**

### A. Water Recovery Model

We implemented the closed-loop water recovery system as a feedback cycle that extracts water from the exhaust stream and injects it upstream of the HPC. We chose this injection location based on claims from a study by NASA, Boeing, and Rolls-Royce [2] that water injection directly into the combustor is unnecessary. The water vapor recovery component sits downstream of the LPT and extracts water from the flow before exiting the core nozzle. We assume that

a fraction of the total water available in the exhaust stream is recovered and that there are no pressure or temperature losses associated with this process. The component flow interface and mechanical connections, including the water injector and water extractor, are depicted in Figure 2.

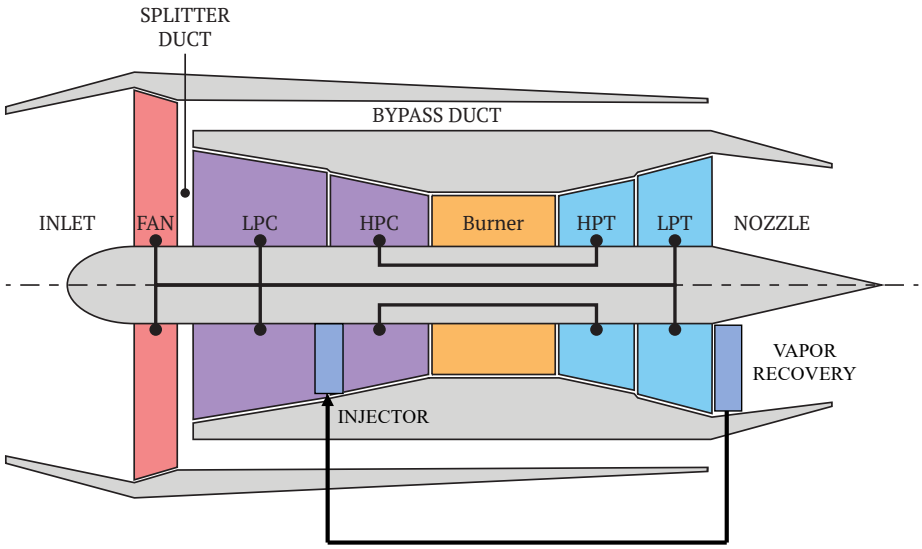


**Fig. 2 The configuration of a high-bypass turbofan model with an integrated closed-loop water vapor recovery and injection system. The water vapor recovery system (extractor) extracts a fraction of the water in the core stream and re-injects it upstream of the high-pressure compressor. This diagram illustrates the feedback effect that this implementation has on the overall core flow.**

To account for the humidity of the inlet air as well as the increased humidity after water injection, we modified the composition of the air mixture upstream of the combustor. pyCycle provides a `wet-air` dataset that introduces $H_2O$ molecules to the composition of air. We prescribe atmospheric mass-specific humidity as a water-to-air ratio (WAR) that is defined as the ratio of $H_2O$ to air in the reactants of the inflow mixture. Kalnay et al. [12] give the humidity values for each flight condition and are shown in Table 1.

We introduce two new thermodynamic models for water recirculation in pyCycle. A water injector adds water to the flow upstream of the HPC, while a water extractor diverts a portion of the water in the flow away from the exhaust stream. The injector operates similarly to fuel injection in the pyCycle combustor component. We determine a WAR that is analogous to the fuel-to-air (FAR) ratio in the combustor. This WAR is used to compute the chemical species present in the flow at the current thermodynamic state, determined by the incoming flow. The new species composition and thermodynamic state are determined using the pyCycle CEA solver [9]. The water injector inputs are the mass flow rate and mass fraction of water. We can solve for the mass flow rate on a mixture basis using the WAR, or directly by specifying the mass flow rate of water. A schematic of the injector is shown in Figure 3a where $Y_{H_2O}$ is the mole fraction of water molecules.

The water extractor model diverts a fraction of a specific species from one flow path to another. The CEA solver calculates the inflow composition and the extractor separates a specific species based on a mass fraction input. The composition of the core stream is updated to represent the remaining mixture after the extractor model removes the species from the incoming flow. We then solve for the thermodynamic state and flow path areas at the outflow of both extractor streams. A simple schematic of the extractor is shown in Figure 3b where $Y_{H_2O}$ is the mole fraction of water molecules and $X_{H_2O}$ is the fraction of water that is recovered from the core stream. We connect one outflow stream of the extractor to the inflow stream of the injector to complete the water recirculation system. The model results in a mismatch between the mass flow rate upstream of the HPC and the mass flow rate exiting the core nozzle. To preserve conservation of mass, we treat the water recirculation as a nonlinear cycle that must converge before the engine calculation is physically balanced. In this model, we are assuming the water molecules are removed from the exhaust stream with no pressure or temperature losses. We also assume the injected water molecules are at the same pressure and temperature as the air flow just before the HPC. We illustrate the water recirculation loop and the nonlinear solver

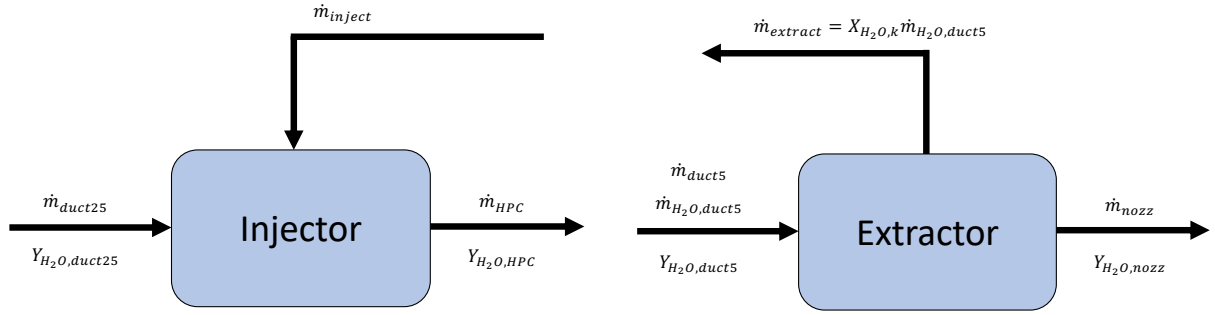


**(a) Water from the extractor is simply injected into the core flow upstream of the high-pressure compressor.**

**(b) We extract a fraction of the moles of water from the out flow of duct 5. The extracted water is routed back upstream to the injector and the rest is exhausted out the nozzle.**

**Fig. 3 Injector (left) and extractor(right) diagrams that show the inputs and output streams of each component. The inputs and outputs show which flow values are used to compute the amount of recirculated water.**

connections in Figure 5.

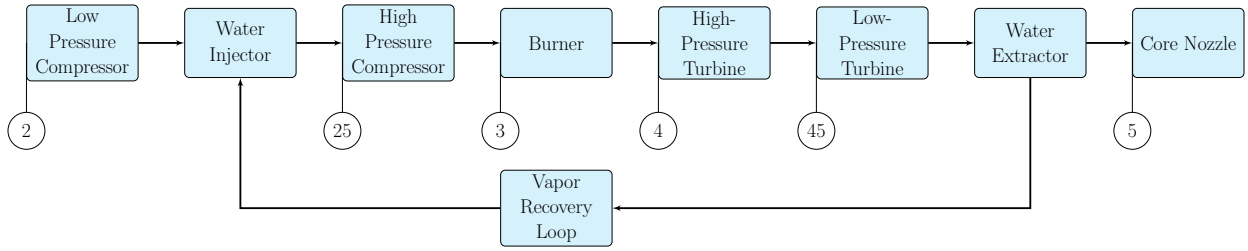


**Fig. 4 Simplified layout of the N+3 engine cycle with the closed-loop vapor recovery. Black arrows are flow connections, blue boxes are cycle elements. Flow stations are identified with bubble text.**

### B. Multipoint Propulsion Model

The N+3 model is a collection of components that combine to form a unified zero-dimensional cycle. The model consists of twenty-five different elements that define the flow path and the mechanical systems. Thermodynamic quantities are solved and exchanged using CEA at flow path boundaries represented by black arrows between blue flow path components in Figure 1. The fan, gearbox, low pressure, and high pressure systems are connected by three mechanical shafts depicted in red in Figure 1.

We operate the engine cycle in different modes depending on the desired conservation relationships, design rules, and flight conditions. In "on-design" mode, we prescribe cycle inputs such as turbo machinery efficiencies, pressure ratios, and combustion temperatures. The "off-design" mode inherits the flow path areas and turbo machinery map scalars from the "on-design" analysis.

We impose *balance* equations to satisfy the physical governing equations, conservation laws, and design rules. *Balance* relationships are formulated as equations in the form $r(u) = 0$ where $r$ is a residual function and $u$ is an implicit state variable. We use Newton based solvers to find the value of the state variables that drive the set of balance residuals to zero. Hendricks and Gray provide the extensive set of balance equations with further details on the construction of the nonlinear system for the N+3 model.

The "on-design" point is top-of-climb (TOC) with "off-design" conditions at rolling takeoff (RTO), sea-level static (SLS), and cruise (CRZ). To account for each of these operating conditions, the N+3 model uses a technique called Multipoint Design Point (MDP) modeling to converge the model to an engine design. Table 1 shows the different altitudes and mach numbers for each flight condition. We consider these points because they either limit the performance at cruise or present critical design considerations for the propulsion system. The design rules at SLS ensure that the

**Table 1 Altitude and mach numbers at each of the flight conditions considered in the multipoint formulation. The humidity ratios were computed from humidity data [12].**

| Parameter | TOC | RTO | SLS | CRZ | Units |
|---|---|---|---|---|---|
| Altitude | 35000 | 0 | 0 | 35000 | ft |
| Mach | 0.8 | 0.25 | 0.0 | 0.8 | - |
| Humidity Ratio | 0.00017 | 0.009 | 0.009 | 0.00017 | kg/kg |

turbo machinery and flow paths meet the static thrust target. Rolling takeoff limitations constrain the upper limit of the combustor temperature and subsequently the cooling requirements of the turbines. The cooling mass flow rates ($\dot{m}_{\text{cool,k}}$) are passed from the RTO point to all other flight conditions creating a cyclic connection. We add a fuel burn objective at cruise to optimize the engine performance during the longest flight segment. We size the water recovery system at the CRZ condition because it has the greatest impact on fuel burn over the flight envelope. Similarly to $\dot{m}_{\text{cool,k}}$, the water recovery mass flow rates ($\dot{m}_{\text{water,k}}$) are connected back to the other operating points. The interconnections between flight conditions create a complex nonlinear loop, shown in Figure 5. The converged model represents a feasible multipoint engine that accounts for design considerations and conservation laws at all four operating conditions. We direct the reader to the N+3 multipoint model definition in the paper by Hendricks and Gray [8] for the detailed description of the balance relationships.

## III. Optimization Problem

We performed multipoint gradient-based design optimization of the N+3 engine model considering the TOC, RTO, SLS, and CRZ flight conditions. The objective is to minimize fuel burn subject to design and performance constraints.

Typical gas-turbine analysis measures the efficiency using the thrust-specific fuel consumption (TSFC). However, this metric is not useful in the comparison of efficiency between Jet-A and hydrogen fueled cycle models because of the differences in fuel density and energy capacity. A better metric for comparing Jet-A versus hydrogen is thrust-specific energy consumption (TSEC) [1]. TSEC is TSFC multiplied by the lower heating value (LHV) of the fuel shown in Equation (2).

$$\text{TSFC} = \frac{\dot{m}_{\text{fuel}}}{F_{\text{thrust}}} \tag{1}$$

$$\text{TSEC} = \frac{\dot{m}_{\text{fuel}}\text{LHV}}{F_{\text{thrust}}} = \text{TSFC} \times \text{LHV} \tag{2}$$

For this work we are concerned with minimizing fuel burn of the engine subject to known thrust constraints. TSEC will be used as a efficiency metric at the cruise condition to compare the two fuels in the results. The fuel properties used in the engine model are given in 2.

**Table 2 N+3 model fuel properties. The lower heating values are given for each fuel used to compute TSEC.**

| Parameter | Value | Units | Description |
|---|---|---|---|
| $\text{LHV}_{\text{JetA}}$ | 18564.0 | BTU/lbm | Lower heating value of Jet-A * |
| $\text{LHV}_{\text{H2}}$ | 51591.0 | BTU/lbm | Lower heating value of H2 † |

Large multidisciplinary optimization problems are commonly represented with extended design structure matrix (XDSM) diagrams. XDSM diagrams are used to visualize the complex implicit and explicit relationships between functions, the solver, and optimizer. An XDSM diagram of the optimization problem with the multipoint formulation is shown in Figure 6.

The design variables for this problem are pressure controls such as fan pressure ratio ($\text{PR}_{\text{fan,TOC}}$), low pressure compressor pressure ratio ($\text{PR}_{\text{LPC,TOC}}$), overall pressure ratio at CRZ ($\text{OPR}_{\text{TOC}}$). Other design variables are temperature controls such as burner temperature at RTO ($T_{4,\text{RTO}}$) and the TOC-RTO burner temperature ratio ($T_{4,\text{ratio}}$). TOC-to-RTO burner temperature ratio ($T_{4,\text{ratio}}$) is shown in Equation (3).

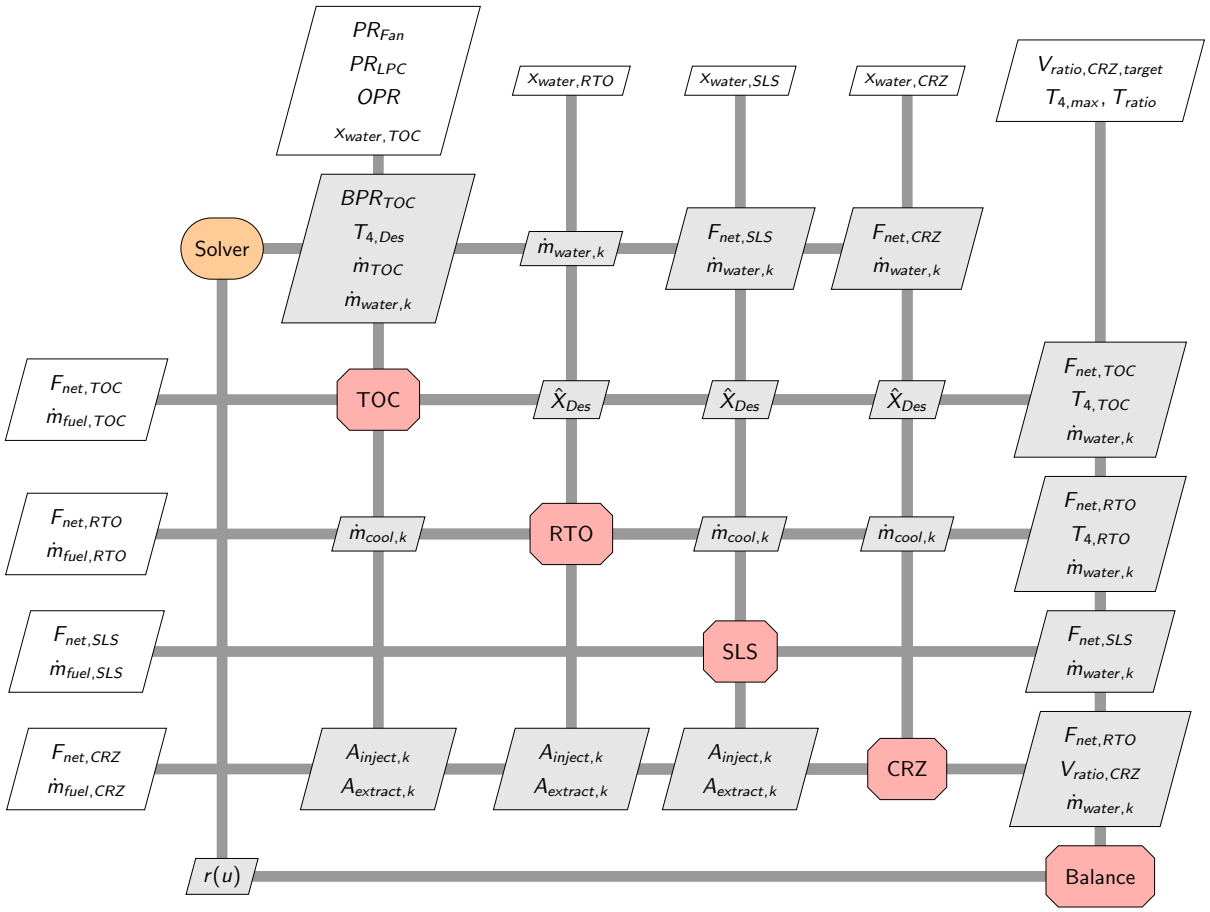


**Fig. 5 Full multidisciplinary design analysis (MDA) model N+3 XDSM diagram. This XDSM diagram shows the multipoint coupling between the different operation conditions and shows how the water recovery fractions are used to solve for water mass flow rates.**

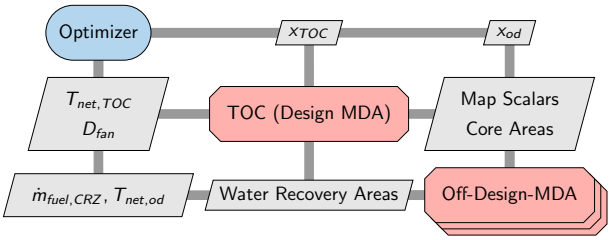


**Fig. 6 XDSM diagram of the multipoint optimization problem with objective, constraints, and MDA block. The XDSM diagram shows the variables and outputs within the optimization model and how each of these values is connected to the optimizer and MDA block.**

$$T_{4,\text{ratio}} = \frac{T_{4,\text{TOC}}}{T_{4,\text{RTO}}} \tag{3}$$

The nozzle velocity ratio at CRZ ($V_{\text{ratio,CRZ}}$) is also added as a design variable to control the bypass ratio and mass flow rate through the engine. The nozzle velocity ratio is defined as,

$$V_{\text{ratio}} = \frac{V_{\text{core,ideal}} C_{v,\text{core}}}{V_{\text{bypass,ideal}} C_{v,\text{bypass}}} \tag{4}$$

where $V_{ideal}$ is the exit velocity of a nozzle and $C_v$ is the velocity coefficient which accounts for non-ideal effects. Finally, the water recovery fraction at CRZ ($X_{\text{H}_2\text{O,CRZ}}$) is added as a design variable in order to take advantage of water recirculation. We only add the water recovery fraction at CRZ as a design variable since we are optimizing $\dot{m}_{\text{fuel,CRZ}}$. The CRZ operating condition is also the longest flight segment and therefore contributes the most to long-term performance.

The net thrust for the SLS and CRZ conditions are set using *balance* components. Net thrust for SLS is constrained to be 1.2335 times the net thrust at RTO which itself is constrained to 22800 lbf. Similarly, the net thrust at CRZ is constrained to be 0.9 times the net thrust at TOC. The bypass ratio (BPR) at TOC is set by the *balance* component such that the CRZ nozzle velocity ratio meets a given target value. The CRZ velocity ratio constraint ensures that the core exit velocity is higher than the bypass exit velocity. The TOC engine mass flow rate is set by the *balance* component using the combustor temperature at RTO, $T_{4,\text{RTO}}$.

The optimization problem objective function, design variables, and constraints are shown in Table 3. The thermodynamic cycle design variable ranges are determined from the expected N+3 technology limits [8]. Additionally, the design variable ranges are shown in Table 4.

**Table 3 Multipoint optimization problem definition. The objective function is the thrust specific energy consumption at the cruise condition. The constraints are net thrust and engine diameter constraint at the design point, TOC.**

| | Variable/Function | Description | Units | Quantity |
|---|---|---|---|---|
| minimize | $\dot{m}_{\text{fuel,CRZ}}$ | Fuel flow rate at CRZ | lbm/s | 1 |
| with respect to | $X_{\text{H}_2\text{O,CRZ}}$ | Water recovery mass fraction at CRZ | - | 1 |
| | $\text{PR}_{\text{fan,TOC}}$ | TOC fan pressure ratio | - | 1 |
| | $\text{PR}_{\text{LPC,TOC}}$ | TOC low-pressure compressor pressure ratio | - | 1 |
| | $\text{OPR}_{\text{TOC}}$ | TOC overall pressure ratio | - | 1 |
| | $T_{4,\text{RTO}}$ | RTO combustor temperature | °R | 1 |
| | $T_{4,\text{ratio}}$ | TOC-to-RTO temperature ratio (Equation (3)) | - | 1 |
| | $V_{\text{ratio,CRZ}}$ | Core-to-bypass nozzle velocity ratio at CRZ (Equation (4)) | - | 1 |
| | | Total | | 7 |
| subject to | $F_{\text{net,TOC}} \geq 5800.0$ | Target net thrust at TOC | lbf | 1 |
| | $D_{\text{fan}} \leq 100$ | Maximum Fan Diameter | $\text{inch}^2$ | 1 |
| | | Total | | 2 |

**Table 4 Design variable ranges for the optimization problem.**

| Design Variable | Lower | Upper | Units |
|---|---|---|---|
| $X_{\text{H}_2\text{O,CRZ}}$ | 0.0 | 1.0 | - |
| $\text{PR}_{\text{fan,TOC}}$ | 1.2 | 1.4 | - |
| $\text{PR}_{\text{LPC,TOC}}$ | 2.5 | 4.0 | - |
| $\text{OPR}_{\text{TOC}}$ | 40.0 | 70.0 | - |
| $T_{4,\text{ratio}}$ | 0.5 | 0.95 | - |
| $T_{4,RTO}$ | 3000.0 | 3600.0 | °R |
| $V_{ratio,CRZ}$ | 1.35 | 1.45 | - |

The N+3 pyCycle model is implemented in OpenMDAO [10] to enable multidisciplinary gradient-based optimization with analytic coupled derivatives. We use pyOptSparse [13] to facilitate the use of state-of-the-art optimization software

through a unified python interface. We solve the optimization problem listed in Table 3 with SNOPT [14], a gradient-based sequential quadratic programming (SQP) algorithm for large-scale constrained problems.

During initial optimization studies of this model, it was found that when $T_{4,\mathrm{RTO}}$ and $X_{\mathrm{H_2O,CRZ}}$ are design variables at the same time they had opposite effects on the design. The optimizer increases $X_{\mathrm{H_2O,CRZ}}$ which allows for a lower optimal $T_{4,\mathrm{RTO}}$. This is likely due to the interdependency between engine mass flow rate and $T_{4,\mathrm{RTO}}$. As the recovery water fraction increases less mass flow rate is required through the engine which lowers the required $T_{4,\mathrm{RTO}}$ for a required level of thrust. It was also observed that $X_{\mathrm{H_2O,CRZ}}$ is increased until the model breaks due to the CEA solver not being able resolve the increased $H_2O$ molecules that are injected. Since $T_{4,\mathrm{RTO}}$ would be pushed down to its lower limit, it was set as the optimal value from the optimizations with no water recovery. This allowed the optimizer to find the maximum $X_{\mathrm{H_2O,CRZ}}$ that would allow the most water to be recirculated. The upper bound on $X_{\mathrm{H_2O,CRZ}}$ was found to be around 30% for Jet-A and 17% for $H_2$.

## IV. Results

### A. Optimization Results

The 4 optimizations described in the section III were run and solved. The optimality and feasibility targets for the optimizations was $10^{-6}$. These optimizations took between 20-30 major SNOPT iterations to reach optimality and were completed in approximately 36-48 minutes on a standard laptop. The optimality, feasibility, and merit function for each optimization is shown plotted in Figure 7. From Figure 7 we observe quadratic convergence in the optimality of the problem near the optimal solution as expected. A feasible design is reached and the merit function is reduced to its final value in about 10 iterations for all cases.

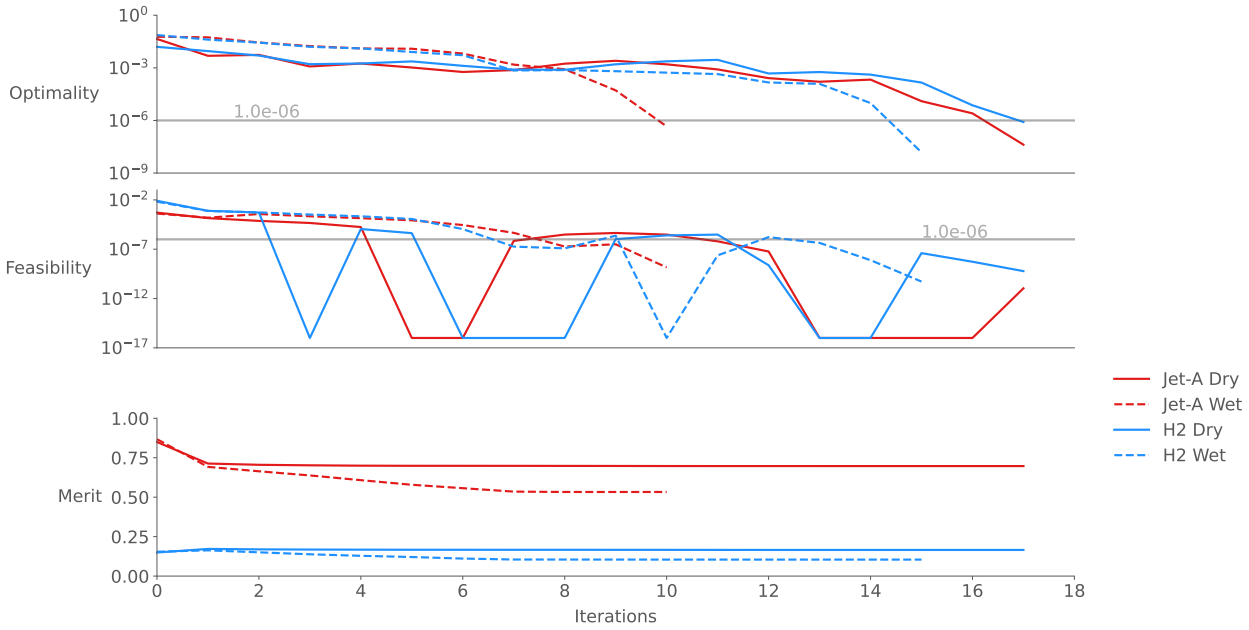


**Fig. 7 The optimality, feasibility, and merit function history for each optimization problem. Jet-A without water recovery is shown with the solid lines, the Jet-A with water recovery is shown with dashed lines, hydrogen without water recovery is shown with dash-dot lines, and hydrogen with water recovery is shown with dotted lines.**

The optimal design variables for each of the four optimizations is shown in Table 5. Note that the $T_{4,\mathrm{RTO}}$ variables are only present for the optimizations without water recovery and the $X_{\mathrm{H_2O,CRZ}}$ variables are present only for the optimizations with water recovery.

The resulting optimal values from the optimization problems are shown in Figure 8 on a parallel coordinate plot. Figure 8 shows the how each of the optimal overall design of the engine compares across fuel type with and without water recovery. We see that across the range of values that each optimal value is very similar with the exception of water recovery fraction. As noted earlier, the water recovery fractions are different because the optimizer pushes $X_{\mathrm{H_2O,CRZ}}$

**Table 5 Optimization results of the N+3 engine for four optimizations using Jet-A and hydrogen fuel with and without water recirculation.**

| | Variable/Function | Jet-A Dry | Jet-A Wet | $H_2$ Dry | $H_2$ Wet | Units |
|---|---|---|---|---|---|---|
| objective | $\dot{m}_{\text{fuel,CRZ}}$ | 0.639 | 0.606 | 0.233 | 0.221 | lbm/s |
| | $\text{TSEC}_{\text{CRZ}}$ | 8186.254 | 7766.338 | 8295.236 | 7859.635 | lbm/hr/lbf |
| variables | $x_{H2O,CRZ}$ | - | 0.3 | - | 0.17 | - |
| | $\text{PR}_{\text{fan,TOC}}$ | 1.285 | 1.292 | 1.288 | 1.297 | - |
| | $\text{PR}_{\text{LPC,TOC}}$ | 4.0 | 4.0 | 4.0 | 4.0 | - |
| | $\text{OPR}_{\text{TOC}}$ | 61.012 | 61.188 | 60.660 | 61.952 | - |
| | $T_{4,ratio}$ | 0.913 | 0.911 | 0.918 | 0.915 | - |
| | $T_{4,RTO}$ | 3220.574 | - | 3204.071 | - | °R |
| | $V_{ratio,CRZ}$ | 1.35 | 1.35 | 1.35 | 1.35 | - |
| constraints | $F_{net,TOC}$ | 5800.0 | 5800.0 | 5800.0 | 5800.0 | lbf |
| | $D_{Fan}$ | 100.0 | 100.0 | 100.0 | 100.0 | $in^2$ |

to the highest value it can attain. The $\text{PR}_{\text{fan,TOC}}$ and $V_{ratio,CRZ}$ design variables go to their upper and lower limits, respectively.

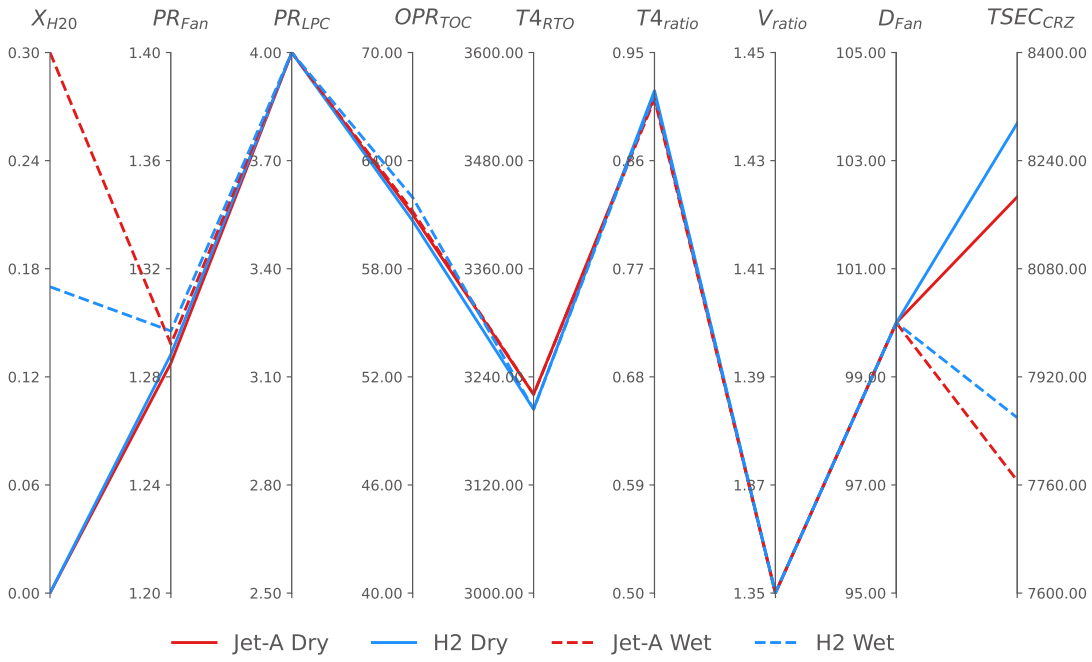


**Fig. 8 Optimization results of the N+3 engine with and without no water recovery using Jet-A and H2 as the fuel. The red lines show Jet-A fuel and the blue lines show $H_2$ fuel. The solid lines show the engine without water recovery and the dashed lines show the engine with water recovery.**

$\text{PR}_{\text{fan,TOC}}$ likely goes to its upper value since its more efficient to increase $\text{PR}_{\text{fan,TOC}}$ than $\text{OPR}_{\text{TOC}}$. $V_{ratio,CRZ}$ tends toward its lower value since the engine is more efficient when the bypass stream is larger and has more mass flow through it. The main differences in the engine designs are the pressure ratios and temperatures. Between the two fuel types, the water recovery fraction for both is pushed up to the upper limit of the design space. One reason the water recovery fraction increases to its upper bound use to improve combustion characteristics of the core flow when fuel is injected. The same thrust output can be achieved with water recovery at a lower FAR, slightly lower temperature,

and less total mass flow rate. The recovery fraction does not directly relate to the mass flow rate of recirculated water since more available water will increase the recirculation flow rate. It is noted that recovery fraction for $H_2$ is smaller than the recovery fraction for Jet-A because there is more water produced in the combustion process. However, the mass flow rate of water is larger for $H_2$ at 0.405 lbm/s as opposed to 0.324 lbm/s for Jet-A. The $H_2$ fuel has the benefit of recovering more water at a lower fraction of the overall water in the core exhaust. We see slightly higher pressure ratios across the fan with water recovery leading to a larger overall pressure ratio. The $T_{4,\text{RTO}}$ value for Jet-A is slightly higher than that of $H_2$. This is most likely due to the combustion properties of $H_2$ compared to Jet-A. $H_2$ can has a wider combustion flammability limit and allows the engine to burn at a lower equivalence ratio to attain the same thrust requirements. Burning leaner not only cools the engine but also reduces fuel consumption. Therefore, TOC temperatures are colder with the $H_2$ fuel and even slightly colder when adding water recovery. The engine is likely able to size the components with water recovery so that the same thrust is generated at a lower fuel-to-air ratio. Furthermore, adding water recovery at CRZ slightly decreases the $T_{4,\text{ratio}}$ value. As noted earlier, the water recovery and injection allows the engine achieve the same level of thrust at a lower temperature. In terms of pressure ratios we see that the fan pressure ratio increases with hydrogen fuel and even more with water recovery. This is again likely due to using $H_2$ and water recovery each resizing the engine to increase the amount of thrust generated by the fan. The breakdown of the gross thrust fractions from the core and bypass nozzles for each point is shown in Table 6. Table 6 shows that the fraction of gross thrust generated by the core nozzle decreases when we use $H_2$ and decreases further when adding water recovery. Utilizing the fan more than the core nozzle increases the efficiency of the engine since we are not burning as much fuel but is limited by the maximum size of the fan. The increase in $\text{OPR}_{\text{TOC}}$ mostly reflects the increase in $\text{PR}_{\text{fan,TOC}}$ and resizes of the turbojet section of the engine with water recovery.

**Table 6 Thrust breakdown for each flight operating condition. The net thrust, gross thrust, and ram drag are shown for each optimization result.**

| Point | Thrust Fraction | Jet-A Dry | Jet-A Wet | H2 Dry | H2 Wet |
|---|---|---|---|---|---|
| TOC | Core | 6.47% | 6.05% | 5.95% | 5.47% |
| | Bypass | 93.53% | 93.95% | 94.05% | 94.53% |
| RTO | Core | 6.31% | 5.87% | 5.77% | 5.26% |
| | Bypass | 93.69% | 94.13% | 94.23% | 94.74% |
| SLS | Core | 6.11% | 5.68% | 5.58% | 5.09% |
| | Bypass | 93.89% | 94.32% | 94.42% | 94.91% |
| CRZ | Core | 6.02% | 5.42% | 5.53% | 4.71% |
| | Bypass | 93.98% | 94.58% | 94.47% | 95.29% |

The $\text{TSEC}_{\text{CRZ}}$ improvement due to water recovery relative to no water recovery for both fuels is shown on a bar chart in Figure 9.

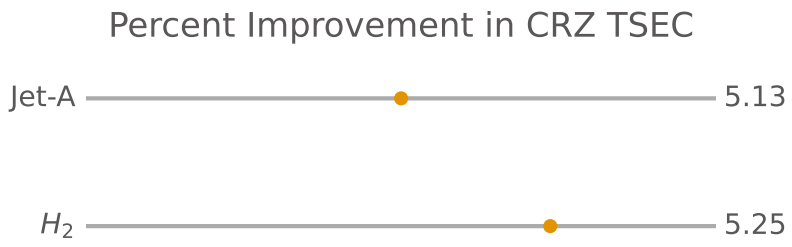


**Fig. 9 Percent relative improvement in thrust specific energy consumption (TSEC) of the N+3 engine with water recovery. This plot compares the relative improvement of the two optimization problems with water recovery compared to the optimization problems without water recovery.**

We see an improvement greater than 5% at CRZ for TSEC for both fuels. Given that most of the design variables change only slightly between designs, most of the efficiency gains are driven by water recovery and injection. This level

of improvement would have a significant reduction in fuel costs over the course of an engine's lifecycle. As Ström and Gierens points out, the water in the exhaust of a $H_2$-powered engine would have close to 3 times the amount of a similar Jet-A engine. Due to the comparatively small amount of water in the exhaust stream for Jet-A, the Jet-A engine would require a larger condenser with more surface area. Therefore, $H_2$ is a much more appealing fuel to use with the proposed closed-loop water recovery system.

### B. Condenser Design Space Study

The large efficiency improvement gained from water recirculation warrant a study of a condenser that could be developed to capture these gains. Companies that are developing engines with water recirculation suggest that hydrogen can be used to as the heat sink for a water condenser [5]. To motivate water recirculation technology it of interest to explore the design space for a condenser designed to fit inside the exhaust stream of a turbofan engine. A relatively low pressure loss condenser would need to be developed for the water recirculation loop to be implemented. pyCycle handles pressure losses in ducts by specifying a pressure loss coefficient, dPqP. This pressure loss coefficient represents is the total pressure loss relative to the inlet pressure of the duct. We varied the total pressure loss across the extraction model to simulate drag from an increasingly large condenser. The rest of the engine design variables were optimized during this pressure loss sweep to determine the how the optimal amount of water recovery changed based on drag losses from the condenser. Figure 10a shows $TSEC_{CRZ}$ of this sweep relative to and engine with no water recovery.

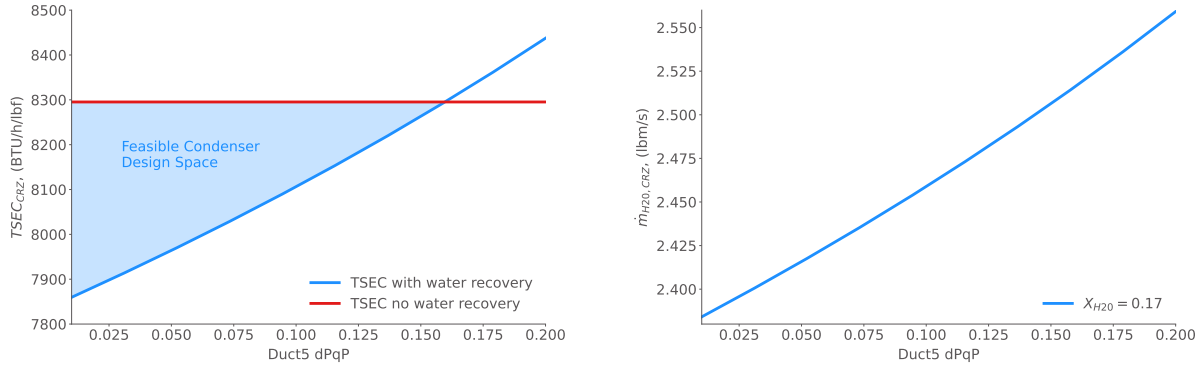


**(a) Pressure loss sweep of Duct5 which is just upstream of the water vapor extractor component. The figure shows the optimized TSEC values for varying levels of pressure loss due to the condensation of water compared to the optimization problem without water recovery. This shows the working space available for designing a water condenser while still gaining the benefits of water recovery.**

**(b) Pressure loss sweep of Duct5 which is just upstream of the water vapor extractor component. The figure shows the resulting total available water in the exhaust stream for varying levels of pressure loss in the extractor flow path. The engine was optimized with the water recovery upper bound of 17%.**

**Fig. 10**

From Figure 10a, we can see the design space in which the closed-loop water recovery model is feasible. The water recovery model will offer efficiency improvements up until about dPqP = 0.16. A value of dPqP = 0.16 means that a 16% loss of pressure from the condenser is allowed assuming the maximum water recovery fraction of 17% for $H_2$. This improvement design space would be reduced if only a smaller fraction of water recovered could be obtained. The total water available in the core stream as a function of the same pressure loss is shown in Figure 10b. Figure 10b shows that the optimizer finds designs that increase the available water in the core stream. Since the water recovery fraction is always pushed to 17%, the water mass flow rate that is recovered increases to overcome the pressure loss. This effect helps the engine increase the feasible design space in Figure 10a.

## V. Conclusion

In this paper, we describe a novel closed-loop water recirculation system for commercial aviation engines. The water recirculation system was designed and implemented into the N+3 ultra-high bypass engine model. We have presented

the results of four optimization problems demonstrating the use of this technology using the pyCycle cycle modeling tool for Jet-A and hydrogen fuel.

The recirculation system is implemented by introducing two new custom pyCycle components, the water extractor and injector, which form a continuous closed-loop feedback water flow in the engine. We then described the multipoint design problem and how it is used to design an aircraft engine to meet the operating requirements at different flight regimes. The optimization problem is then introduced with constraints on the thrust and overall engine size at the design point. The design variables used are thermodynamic design variables describing the temperatures, pressures, and velocities within the engine. An additional design variable controlling how much water is recirculated is added at the cruise point to improve the fuel burn. The optimization problem was solved for four cases: with Jet-A or hydrogen fuel, and with or without water recirculation.

The results from the optimization problems show temperature, thrust, and efficiency improvements when using hydrogen as a fuel and even further improvements with water circulation. Thermal reductions with hydrogen and water recirculation will improve the lifetime of the engine which would reduce maintenance and overall costs. Between the two fuels, we see similar values of the engine performance metric, TSEC. Significant energy efficiency gains are seen with water recirculation which would improve the overall costs of the engine during its operational lifecycle. At the same water recovery fraction, hydrogen with water recirculation could achieve a lower TSEC value.

There are technological obstacles to overcome in order to implement this water recirculation system in a modern turbofan engine. The main obstacle would be how to design a condenser that can recover a portion of the exhaust water without a excessive drag pressure losses. Therefore, a condenser design space study was completed to show the feasible design space for such a condenser. The results showed that at the maximum possible water recovery fraction for hydrogen quite a large pressure loss can be imposed before the improvements are canceled out. Furthermore, using hydrogen as the fuel allows for designs that are not available for an engine using Jet-A. The thermal properties of hydrogen provide a heat sink and thus a readily available resource for water condensation within the condenser. The hydrogen fuel absorbs heat and is then used in the combustion process, further improving engine efficiency. The novel water recovery system with shows promising efficiency results when used with hydrogen fuel. This water recovery system provides a potential avenue for hydrogen engine design that could help overcome the technological issues associated with hydrogen as a fuel.

## VI. Acknowledgements

We would like to thank Justin Grey for his help with the pyCycle components of this work. Justin's expertise and knowledge of pyCycle tool helped make the development of the custom pyCycle components possible.

## References

[1] Adler, E. J., and Martins, J. R. R. A., "Hydrogen-Powered Aircraft: Fundamental Concepts, Key Technologies, and Environmental Impacts," *Progress in Aerospace Sciences*, 2023. (Under review).

[2] Daggett, D. L., Fucke, L., Hendricks, R. C., and Eames, D. J., "Water Injection on Commercial Aircraft to Reduce Airport Nitrogen Oxides," Tech. rep., NASA, March 2010.

[3] Mourouzidis, C., Igie, U., Pilidis, P., and Singh, R., "WATER INJECTION ON AIRCRAFT ENGINES: A PERFORMANCE, EMISSIONS AND ECONOMIC STUDY," 2015.

[4] Ström, L. J., and Gierens, K., "First simulations of cryoplane contrails." *Journal of Geophysical Research*, Vol. 107, 2002. doi:10.1029/2001JD000838.

[5] "E project: Hydrogen Steam and inter-cooled turbine engine (HySITE)," , Nov 2021. URL `https://arpa-e.energy.gov/technologies/projects/hydrogen-steam-and-inter-cooled-turbine-engine-hysite`.

[6] Gordon, S., and McBride, B. J., "Computer Program for Calculation of Complex Chemical Equilibrium Compositions, Rocket Performance, Incident and Reflected Shocks, and Chapman-Jouguet Detonations," *NASA Rept. RP-1311*, 1994.

[7] Jones, S., *An Introduction to Thermodynamic Performance Analysis of Aircraft Gas Turbine Engine Cycles Using the Numerical Propulsion System Simulation Code*, NASA, 2007. TM-2007-214690.

[8] Hendricks, E. S., and Gray, J. S., "pyCycle: A Tool for Efficient Optimization of Gas Turbine Engine Cycles," *Aerospace*, Vol. 6, No. 87, 2019. doi:10.3390/aerospace6080087.

[9] Gray, J. S., Chin, J., Hearn, T., Hendricks, E., Lavelle, T., and Martins, J. R. R. A., "Chemical Equilibrium Analysis with Adjoint Derivatives for Propulsion Cycle Analysis," *Journal of Propulsion and Power*, Vol. 33, No. 5, 2017, pp. 1041–1052. doi:10.2514/1.B36215.

[10] Gray, J. S., Hwang, J. T., Martins, J. R. R. A., Moore, K. T., and Naylor, B. A., "OpenMDAO: An open-source framework for multidisciplinary design, analysis, and optimization," *Structural and Multidisciplinary Optimization*, Vol. 59, No. 4, 2019, pp. 1075–1104. doi:10.1007/s00158-019-02211-z.

[11] Jones, S. M., Haller, W. J., and Tong, M. T., "An N+3 Technology Level Reference Propulsion System," Tech. Rep. NASA/TM—2017-219501, NASA Glenn Research Center, 2017. URL `https://ntrs.nasa.gov/citations/20170005426`.

[12] Kalnay, E., Kanamitsu, M., Kistler, R., Collins, W., Deaven, D., Gandin, L., Iredell, M., Saha, S., White, G., Woollen, J., Zhu, Y., Chelliah, M., Ebisuzaki, W., Higgins, W., Janowiak, J., Mo, K. C., Ropelewski, C., Wang, J., Leetmaa, A., Reynolds, R., Jenne, R., , and Joseph, D., "The NCEP/NCAR 40-Year Reanalysis Project." *Bulletin of the American Meteorological Society*, Vol. 77, 1996, pp. 437–471.

[13] Wu, N., Kenway, G., Mader, C. A., Jasa, J., and Martins, J. R. R. A., "pyOptSparse: A Python framework for large-scale constrained nonlinear optimization of sparse systems," *Journal of Open Source Software*, Vol. 5, No. 54, 2020, p. 2564. doi:10.21105/joss.02564.

[14] Gill, P. E., Murray, W., and Saunders, M. A., "SNOPT: An SQP Algorithm for Large-Scale Constrained Optimization," *SIAM Review*, Vol. 47, No. 1, 2005, pp. 99–131. doi:10.1137/S0036144504446096.